ISSN: 2093-5374 / E-ISSN: 2093-5382

Design and Analysis of a Nested Triangular Microstrip Bandpass Filter for Multiband Wireless Applications

Mustafa Abd Al-Aress Jabur[1], Rami Qays Malik[2], Zahraa Hashim Kareem[3], Aqeel H. Al-Fatlawi[4*], Ahmed R. Mathloom[5], and Amjed Abbas Ahmed[6]

[1]Department of Computer Techniques Engineering, Imam Al-Kadhim University College (IKC), Baghdad, Iraq. mustafa.abd@iku.edu.iq, https://orcid.org/0009-0006-5066-8545

[2]Medical Instrumentation Technique Engineering Department, College of Engineering and Technologies, Al-Mustaqbal University, Hillah, Babil, Iraq. rami.qays@uomus.edu.iq, https://orcid.org/0000-0003-2518-9260

[3]Medical Instrumentation Technique Engineering Department, College of Engineering and Technologies, Al-Mustaqbal University, Hillah, Babil, Iraq. zahraa.hashim@uomus.edu.iq, https://orcid.org/0000-0002-8012-063X

[4*]Department of Computer Techniques Engineering, Imam Al-Kadhim University College (IKC), Baghdad, Iraq. aqeelhamzah@iku.edu.iq, https://orcid.org/0000-0002-8989-5271

[5]Department of Physics, College of Education for Pure Sciences, University of Thi-Qar, Thi-Qar, Iraq. ahmedrasool30.eps@utq.edu.iq, https://orcid.org/0000-0002-4987-9445

[6]Department of Computer Techniques Engineering, Imam Al-Kadhim University College (IKC), Baghdad, Iraq; Center for Cyber Security, Faculty of Information Science and Technology, Universiti Kebangsaan Malaysia, Malaysia. amjedabbas@alkadhum-col.edu.iq, https://orcid.org/0000-0001-6069-2967

Received: September 26, 2025; Revised: November 17, 2025; Accepted: December 22, 2025; Published: March 31, 2026

Abstract

This paper discusses the electromagnetic design and optimization of a compact, nested triangular complementary microstrip bandpass filter (BPF) for multiband communication applications. Multi-resonant characteristics and strong stopband performance are attained using nested triangular open-loop resonators manufactured on Rogers RO3003 (εr = 3.0, h = 1.52 mm, copper = 35 μm). Full-wave electromagnetic simulations that were done on AWR Microwave Office showed that there are four primary passbands at 5.31 GHz, 9.14 GHz, 10.0-10.66 GHz and 12.91 GHz. The principle passband BPF achieves very good impedance matching, showing S11 ≈ −39.7 dB and for the ultralow S21 ≈ −0.07 dB there is an insertion loss. There are multiple sharp transmission zeros, one of which is located close to 9.136 GHz due to a mixture of the electric and magnetic couplings. Because of that, they achieved significant out-of-band rejection. The designed filter compactly occupies an area of about 0.04 λg × 0.04 λg, which displays a higher level of miniaturization compared to the tri- and dual-band designs that are known. Effective tuning of the center frequencies, bandwidths and transmission zeros can be made using parametric sets of resonator dimensions, gap size changes and coupling modifications. Insertion loss, return loss, fractional bandwidth, group delay, and VSWR are some of the most important performance metrics that were

Journal of Wireless Mobile Networks, Ubiquitous Computing, and Dependable Applications (JoWUA), volume: 17, number: 1 (March-2026), pp. 170-190. DOI: *10.58346/JOWUA.2026.I1.011*

*Corresponding author: Department of Computer Techniques Engineering, Imam Al-Kadhim University College (IKC), Baghdad, Iraq.

evaluated and compared to previous works to demonstrate the improvements in performance and area reduction. This unique nested triangular configuration of CSRRs ultimately gives rise to an optimally compact, selectivity, low-loss technology suited for WLAN, X-band, Ku-band, and other multiband wireless systems.

Keywords: Nested Triangular Resonator, Complementary Split-ring Resonator (CSRR), Microstrip Bandpass Filter, Multiband Wireless Applications, Transmission Zeros, RO3003 Substrate.

1 Introduction

Multiband bandpass filters have become even more critical in today's multi-mode and multiband wireless communications. This is because these filters allow several wireless instruments to operate simultaneously on different frequency bands. This capability enables integrating legacy wireless standards with newer ones and supports the growing number of wireless applications. This includes 5G and the Internet of Things (IoT) (Pandey et al., 2022; Hasan et al., 2025; Oleiwi & Hasan, 2025). The Legend in figure 1 shows a system block diagram of a typical RF transceiver and describes the function of multiband filters (Muralidharan, 2023; Faouri et al., 2022). Upon receiving, the antenna collects incoming signals, which are filtered by a Band Pass Filter (BPF) to remove unwanted frequencies. The filtered signal is amplified by a Low-Noise Amplifier (LNA) and mixed with a Local Oscillator (LO) to produce an Intermediate Frequency (IF OUT) for simplified processing. When transmitting, an input signal (IF IN) is up-converted by another mixer with the LO, amplified by a Power Amplifier (PA), filtered by BPF, and transmitted through the antenna (Mahendran et al., 2021). This architecture enables selective filtering, noise reduction, and efficient signal transmission and reception.

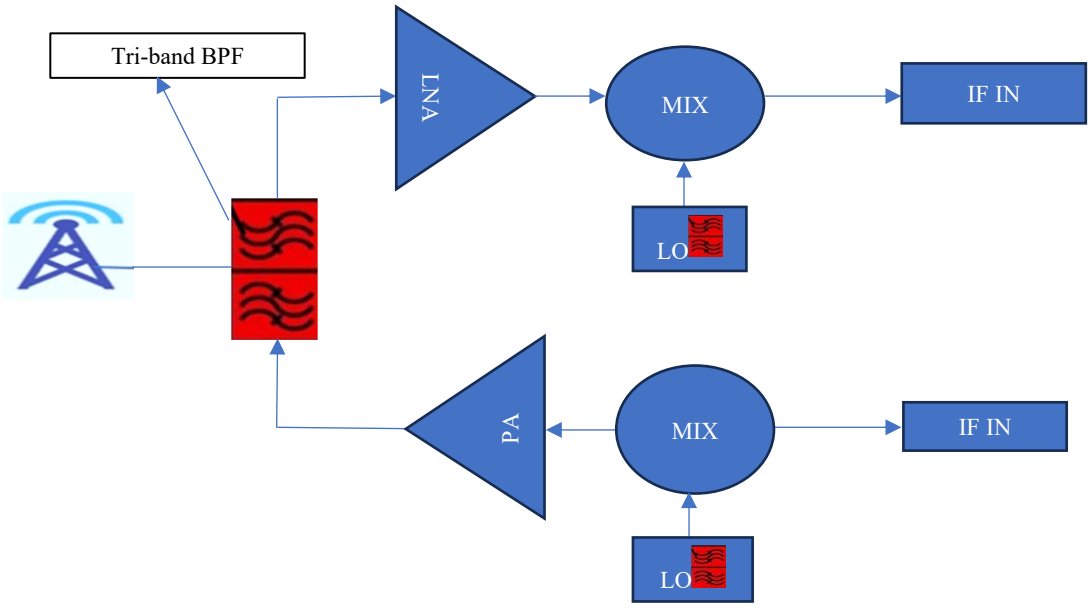

Figure 1: RF transceiver system

Though nonlinear circuitry may introduce unwanted distortion components, there is little to no research on multiband balanced BPFs that address higher-order harmonics generated by nonlinearities (Giji Kiruba et al., 2023; Chidambaram & Rajan, 2025; Hasan et al., 2025). The object of study is the design of tiletable BPFs for rectangular multiband THz (Gari et al., 2024). Coding of the corresponding multiband BPF, i.e., THz, is of utmost importance for the reduction of THz and the efficiency of microstrip circuit design BPF (Ahmed & Almamori, 2025). The inability to switch multiband is a

significant drawback in most wireless systems, BPF (Dawood et al., 2025; George & Iqubal, 2024; Slimani et al., 2022).

Key Contributions

The objective of this study is the design of a compact multiband microstrip bandpass filter based on a nested triangular complementary split-ring resonator (CSRR) structure. This work contributes the following:

- The design and implementation of a novel nested triangular CSRR topology, which, in addition to demonstrating multi-resonant behaviours, also significantly reduced the overall footprint of the structure.
- The ability to improve the passband selectivity by the introduction of additional transmission zeros, which results in enhanced out-of-band rejection.
- The accurate and complete electromagnetic characterization of the structure through the use of full-wave AWR simulations yielding S-parameter results, group delay and fractional bandwidth results, and results through parametric optimization.
- The demonstration of a qualitative comparison with other compact filters in the literature, to show that this structure achieved improved multiband performance with lower insertion loss.
- The filter design and topology are also practical for real-world WLAN, X-band, and Ku-band wireless applications, thus aiding in their ease of fabrication.

This paper is structured as follows: Section 2 presents the theoretical foundation of CSRR geometry and its mathematical formulation. Section 3 contains the simulation configuration, software settings, and the substrate's properties. Section 4 presents the dataset used and the parameter inquiry focused on filter performance. In Section 5, S-parameters, resonant frequencies, and a benchmarking study of related work are also included. Lastly, Section 6 presents the conclusion and outlines possibilities for further investigation.

2 Related Works

The wireless communication industry is seeing advances in filters, duplexers, and triplexers. Doublet and triplexers facilitate filtration and use fiber technology to separate signals for transmission in various functions for the armature. The document presents the most notable works in the field, complemented by studies of the particular works.

The tri-band bandpass filters (TB-BPF) operate on an equilateral triangular SIW resonator. The second and third bands were realized post-perturbation, where coupling restrains resonators to the perturbed triple TM modes of the sidelock, along with the side idle cavities. The introduction of CSRR source-load coupling and strong out-of-circuit existence provides robust out-of-circuit operation, enhancing the technique for sustaining a filter. The construction and operation of a group of dual-wideband balanced BPFs with a wideband branch at 5.55, 7.50, and 8.60 GHz center (Singh et al., 2025; Rehman et al., 2024). The design uses a stubble to coax a flexible transmission of the order, which responds. The construction in 2.53 and 4.60 to 11 I and broad band assignee rejection strong CM (Ren et al., 2021; Rezaei et al., 2022).

A three-band frequency filter is designed using a unique resonator arrangement: a six-mode resonator and a hairpin resonator. This model is designed to be compact while possessing wideband frequency

capabilities. The bands are set to operate at 1.85, 3.5, 4.4, and 5.7 GHz, covering the frequencies used by GSM, WiMAX, and UWB. There is congruence between the fabricated and simulated models, both of which exhibit low return losses and elevated bandwidth. The authors' work, presented in 8 talks, discusses a tri-band microstrip BPF. Open-circuited and short-stub mixes are used. The Q-factor controls and sets the bandwidth and the transmission zeroes. The filter fabricated on an FR4 substrate with a \u03b5r of 4.4 has pass bands at 4.06-4.28, 5.87-6.40, and 14.28-14.58 GHz. The insertion losses are 2.1, 1.35, and 4.08 dB, respectively, for WAS, ISM, and 5G. The proposed triple-mode coaxial resonators are TM010, TE, and TE+ for a wideband BPF by the authors in 9. To further enhance this work, L-shaped feeding probes and a loading disk are used, reducing the overall size by about 80%. Prototypes targeting a centered frequency of 2.5 GHz have a fractional bandwidth of 40% (Basit et al., 2023; Andreica et al., 2024).

We propose a compact triple-band BPF at 1.57, 3.57, and 4.23 GHz, featuring eight transmission zeros for high selectivity, implemented using step-impedance resonators with metallic slot perturbations and an embedded L-shaped structure. We obtained less than 1.2 dB of insertion loss, more than 25 dB of return loss, and more than 15 dB of rejection on a RO4350B substrate suitable for GPS, WiMAX, and satellite applications. In (Ramkumar et al., 2024), a triple-band BPF using quarter-wavelength coupled resonators with transmission zeros was also proposed. In this filter design, four resonators were used, two of which were short-ended quarter-wavelength modified coupled resonators. The proposed filter provides three passbands: 11.67GHz-1.97GHz, 0.2GHz-8.67GHz, and 9.45GHz−10.45GHz, with return loss of 1 dBdB,0.2r 142 2spiand 0.2ely. respectively, design offers nominal square open-loop resonators at 3.65 GHz, suitable for 5G-band communication. In (Slimani et al., 2022), the authors in (Rai et al., 2024) proposed a tri-band balanced BPF using a single stepped-impedance ring resonator (SIRR) with stepped stubs. The design achieves high selectivity, ultra-wide stopband suppression, strong common-mode suppression, and multiple transmission zeros. The common-mode suppression is also strong.

Multi-band microstrip filters have made significant advances in the literature with the use of stepped-impedance resonators (SIRs), substrate integrated waveguides (SIW), split-ring resonators (SRR), and hybrid coupling structures. Although there have been so many reported designs that have been deemed acceptable within the multiband suspension of functionality. They also have been reported to suffer from adverse disadvantages of increased circuit size, greater insertion loss, limited suppression within the stopband, or lack of transmission zeroes (or control of them). Furthermore, many of them have also had the use of composite resonator configurations or stubs, in which case the sluggish scalability is observed. Thus, there is increased demand for compact multiband filter structures with low insertion loss, and design complexity more so on device miniturization. In this case, the nested cistern shaped CSRR also presented within the triangular topology will suit many of the needs of multiband and wireless applications with more selective criteria and greater than average miniaturization (Muhammad & Sohail, 2022).

3 Theoretical Background and Mathematical Description

The operation of the proposed nested triangular complementary split-ring resonator (CSRR) bandpass filter can be described using an equivalent LC resonance model. In CSRR structures, the etched slots behave as series capacitors, while the metallic paths between them act as inductive elements. The fundamental resonant frequency of each nested triangular ring is expressed by equation (1):

$$f_0 = \frac{1}{2\pi\sqrt{L_{eq}C_{eq}}} \quad (1)$$

Where L_{eq} and C_{eq} denote the equivalent inductance and capacitance of the resonator, respectively.

For a CSRR etched on the ground plane, the capacitance is primarily determined by the gap g between the triangular arms, and can be approximated by equation (2):

$$C_{eq} \propto \frac{\varepsilon_{eff} A}{g} \tag{2}$$

Where A is the effective area of the triangular slot, and ε_{eff} is the effective dielectric constant of the substrate.

Similarly, the inductance of the metallic path enclosing the triangular slot is approximated by equation (3):

$$L_{eq} \propto \mu_0 \frac{l_{path}}{w} \tag{3}$$

Where l_{path} is the current path length, and w is the conductor width.

By nesting multiple triangular CSRRs, the structure produces multiple resonant frequencies given by equation (4):

$$f_n = \frac{1}{2\pi\sqrt{L_n C_n}}, \qquad n = 1,2,\dots,k \tag{4}$$

Each nested layer contributes a distinct LC pair, enabling multiband operation.

The transmission zeros (TZs) arise from mixed electric and magnetic coupling between the resonator layers. They can be expressed by equation (5):

$$f_{TZ} = \frac{1}{2\pi\sqrt{(L_m - L_e)(C_m - C_e)}} \tag{5}$$

Where L_m, C_m represent magnetically induced components, and L_e, C_e represent electrically induced components.

The overall ABCD matrix of the filter is obtained by cascading the resonator section with the microstrip feed lines, as shown in equation (6):

$$\begin{bmatrix} A & B \\ C & D \end{bmatrix} = \prod_{i=1}^{N} \begin{bmatrix} A_i & B_i \\ C_i & D_i \end{bmatrix} \tag{6}$$

The S-parameters are finally computed by equation (7):

$$s_{21} = \frac{2}{A + \frac{B}{Z_0} + CZ_0 + D}, s_{11} = \frac{A + \frac{B}{Z_0} - CZ_0 - D}{A + \frac{B}{Z_0} + CZ_0 + D} \tag{7}$$

Where Z_0 is the characteristic impedance of 50 Ω.

This mathematical formulation explains the resonant behaviour, multiband operation, and transmission-zero formation of the proposed filter.

4 Methodology

Recent advances in wireless technology and engineering indicate an ongoing trend for smaller and more efficient integrated fracture and nested resonator systems while retaining utility and flexibility multiband BPFs. Here we provide our efforts to create a nested triangle microstrips resonator from a singular

resonator design to a more complex CSRR configuration where we expect to rely on a more efficient feed line coupling and higher resonant response from the triangle configuration (Mariselvam et al., 2022). Here we present our efforts, using EM simulations, to calculate the S-parameters, VSWR, phase, and group delay to benchmark our designs, shown in figure 2.

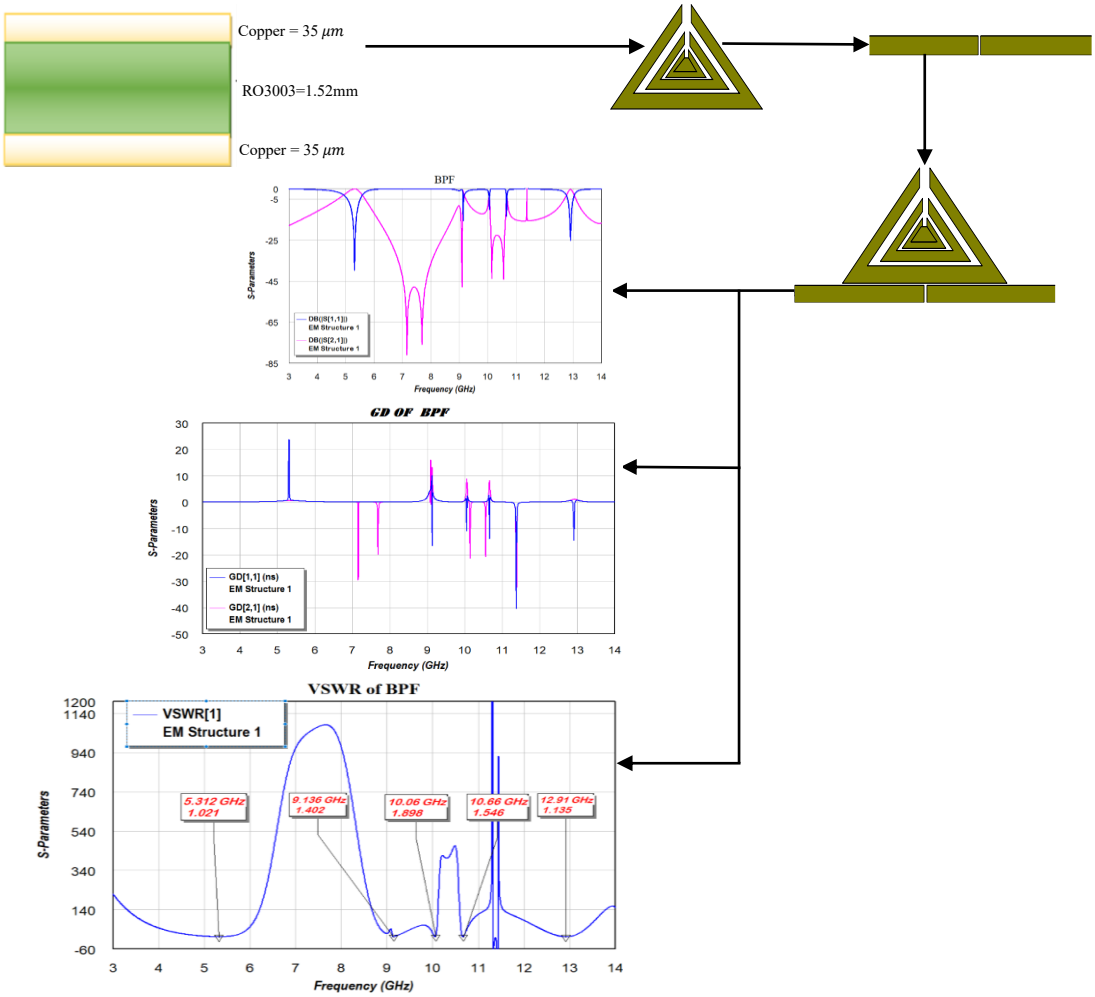

Figure 2: Methodology of the proposed BPF

4.1 Substrate Specifications

In deciding on the substrate type, the first step in the Microstrip BPF design process is to determine the substrate type. This step helps us determine the best strategy for designing a Microstrip BPF. For this substrate, the loss tangent is 0.001, the dielectric constant is 3, the substrate is 1.52 millimeters, and it offers a loss. The Microstrip Technology General Configuration is shown in figure 3.

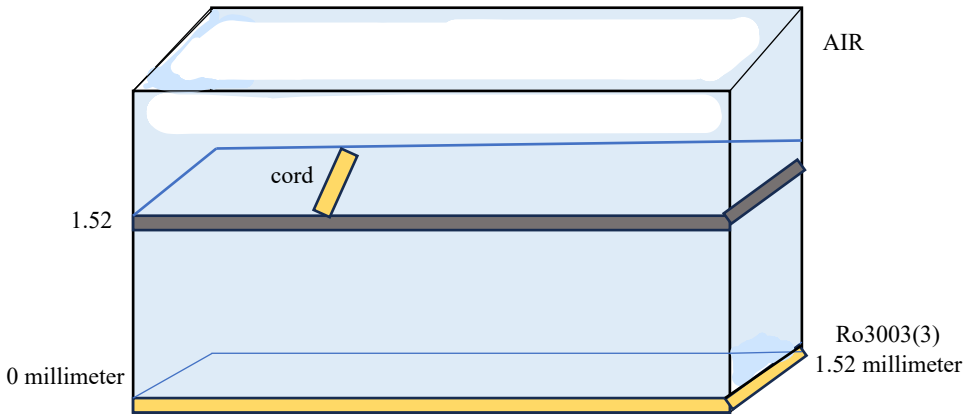

Figure 3: Design a cross-section chart

4.2 Microstrip Transmission Line

4.2.1 Structure of a Microstrip

The basic structure of this Microstrip line is illustrated in figure 4. A Microstrip line is a metal strip with width W and thickness t. This metal strip is located on a dielectric material of height h and relative permittivity εr. In this configuration, a continuous ground plane is located on the bottom of the dielectric substrate.

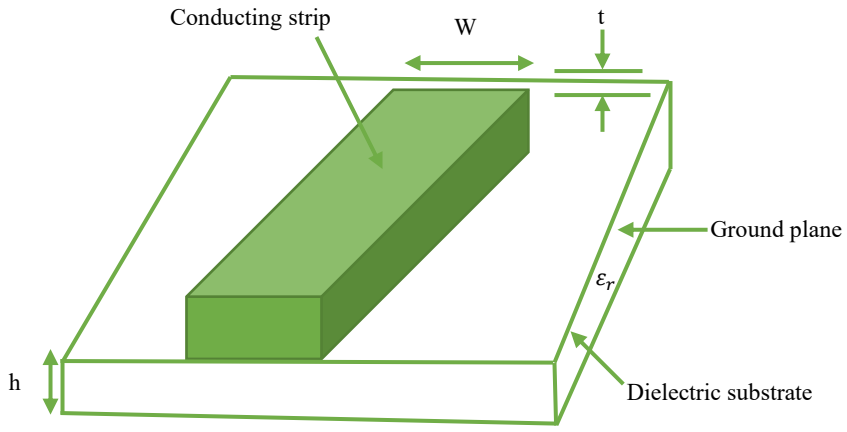

Figure 4: Microstrip line geometry (Weng et al., 2023)

4.2.2 Transmission Line Impedance and Effective Permittivity

The effective dielectric constant and the characteristic impedance chiefly determine the transmission attributes of a Microstrip line. The impact of the line's aspect ratio and the substrate's dielectric constant is dominant at lower frequencies. Microstrip lines are generally considered wider for lower impedance and narrower for higher impedance, with line impedance decreasing at a fixed aspect ratio as the substrate permittivity increases (Yahya et al., 2024).

One of the simplest expressions for determining, under the quasi-TEM approximation, the characteristic impedance of a microstrip line is defined by equation (8) (Mushtaq & Khalid, 2023).

For narrow strips $W/h \leq 1$:

$$\mathbf{ZC} = \frac{60}{\sqrt{\epsilon_{eff}}} \ln\left(\frac{8h}{w} + 0.25\frac{w}{4h}\right) \quad (8)$$

Microstrip ZC, or microstrip characteristic impedance, is measured in ohms. ZC depends on Eeff microstrip properties, such as the effective dielectric constant h and the strip conductor width w.

The equation for determining the microstrip line characteristic impedance is better and applicable to a broader range of parameters. More detail is shown in the lower formula of equation (9). Given ZC estimators are refined to higher precision based on their materials, object properties, and geometry using equations (10), (11), and (12) (Sharma et al., 2024).

For wide strips W/h ≥ 1

$$\mathbf{ZC} = \frac{\mathbf{120\pi}}{\sqrt{\boldsymbol{\epsilon_{eff}}}[\frac{w}{h}+1.393+0.667\ln\left(\frac{w}{h}+1.444\right)]} \quad (9)$$

$$\boldsymbol{\epsilon_r} = \frac{\mathbf{2\epsilon_{eff}-1}}{\mathbf{1}-\frac{\mathbf{2\epsilon_{eff}-1}}{\sqrt{\mathbf{1}+\frac{\mathbf{12h}}{\boldsymbol{w}}}}} \quad (10)$$

For w/h>>1 $\epsilon_{eff} = \frac{\epsilon_r+1}{2} + \frac{\epsilon_r-1}{2}(1+12\frac{h}{w})^{-0.5}$ (11)

If w/h<1 $\epsilon_{eff} = \frac{\epsilon_r+1}{2} + \frac{\epsilon_r-1}{2}(1+12\frac{h}{w})^{-0.5} + 0.04(1-\frac{w}{h})^{-2}$ (12)

Here, t represents the thickness of the strip conductor. These equations apply to microstrip lines with a thin conductor (t" w) and substrates characterized by a relatively low dielectric constant (ϵ_r < 12).

4.3 Resonator Geometry and Topologies

Common resonator configurations in the microstrip bandpass filters are shown in figure 5. In figure 5(a), an uniformly impedance resonator (UIR) is shown, which can provide the fundamental half wavelength resonance. Figure 5(b) shows an example of a conventional half wavelength resonator structure. In figure 5(c), a triangular split ring resonator is shown which is more compact and has favorable modal characteristics for multiband operation. Figure 5(d) shows a stepped impedance resonator (SIR) which has alternate sections of high and low impedance, allowing for the tuning of the resonances and a reduction in size. Thse types of resonators are the primary reason for choosing the triangular CSRR topology used in this work.

The flowchart steps located in figure 6 pertain to the design of the proposed bandpass filter (BPF). It has multiple design options in the AWR program for substrates (RO = 0.001, 3) and (t = 1.52). One application of the design is optimally meant for satellites. For this one, we use 3-14 GHz frequencies and tri-angled resonators as they support multiband applications. A Triangular Open-loop Resonator is a microwave resonator used in various applications, including filters, antennas, and sensing devices. It is a conductive, resonant triangular structure. When we choose to use this variant, we gain the advantage of being more compact at a given resonant frequency than its rectangular or circular counterparts. After we select the appropriate dimensions for the length, width, and the space gap above the triangle, the next important step is to move the energy from the ports to the resonators. In this case, we used two types of ports. The first was SIRs, and the second was UIRs. For the ports, we will choose the final design based on the results. To gain a multiband response, we can use the CSRR method. To wrap it up, we calculated several parameters to evaluate the filter's performance (Insertion loss, Return loss, VSWR, etc.).

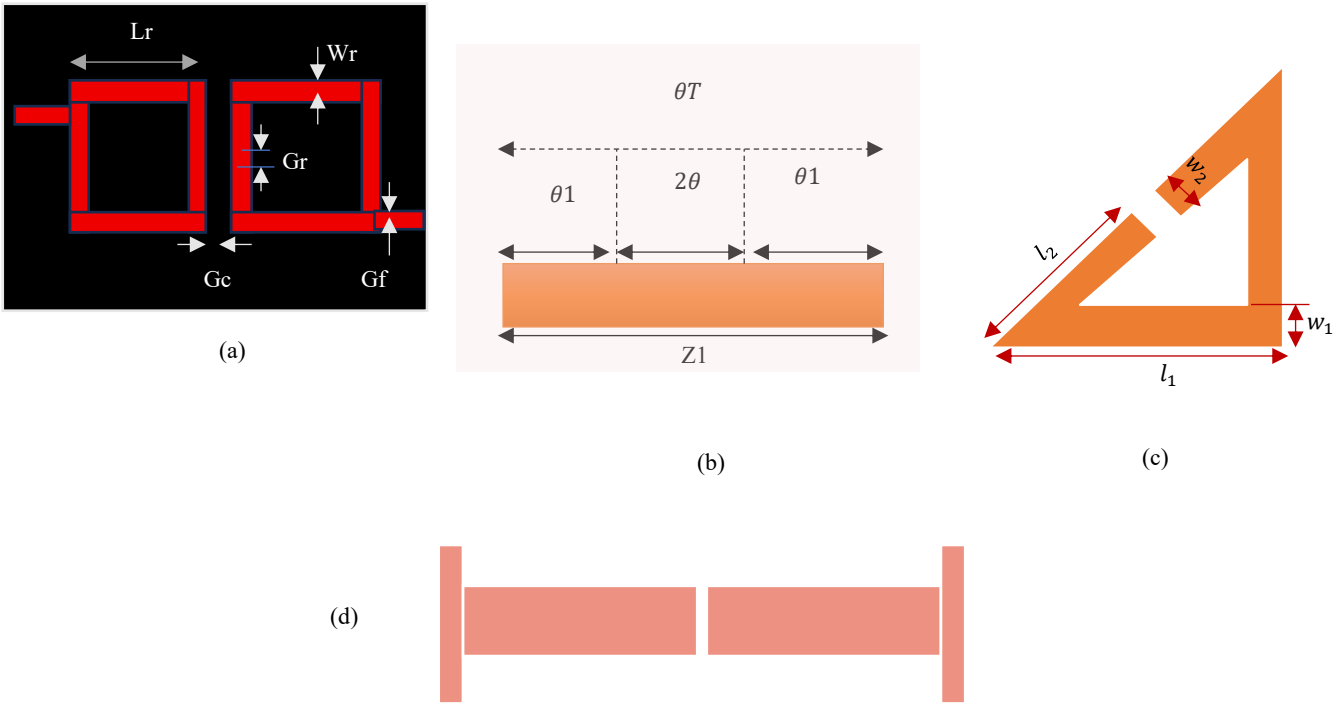

Figure 5: (a) Two split-ring resonators (mezaal & al-zayed, 2019) (UIR), (b) Half-wavelength resonator (pandey et al., 2022) (c) Triangular split resonance ring (balani et al., 2021), (d) SIR (pandey et al., 2022)

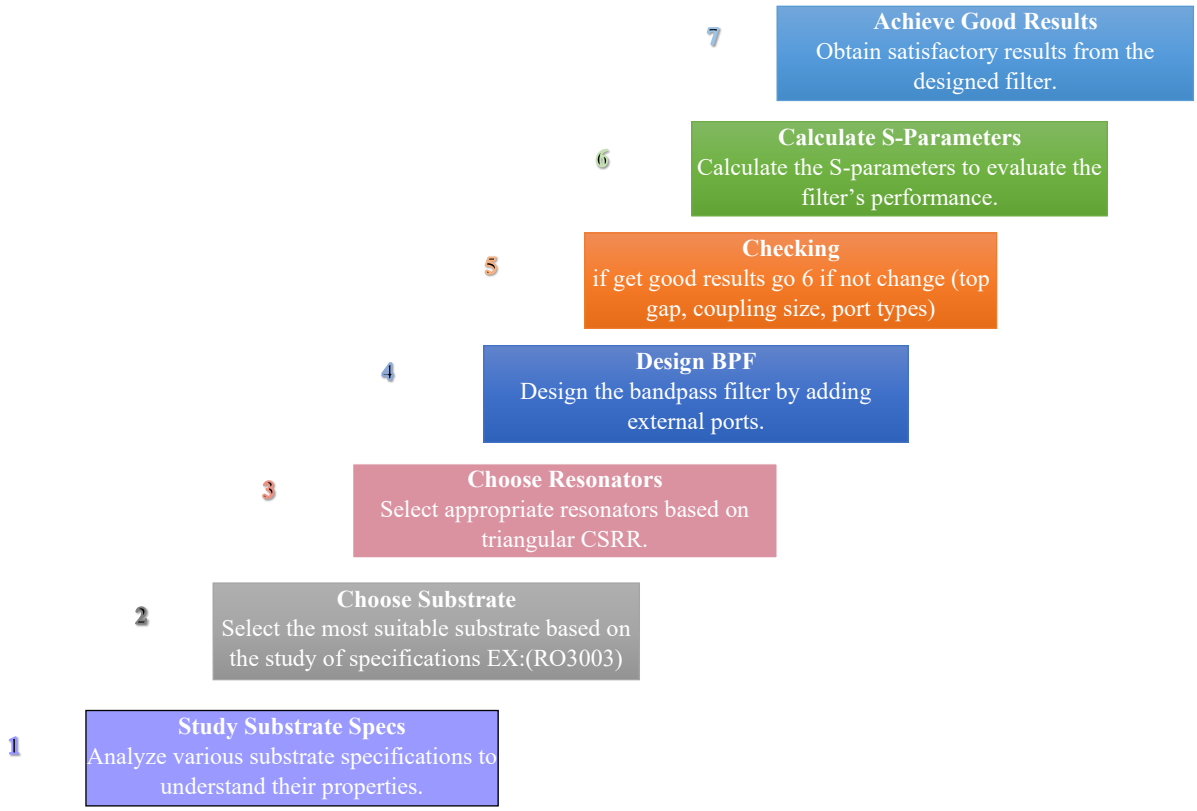

Figure 6: Flow chart and design steps

4.4 Proposed Bandpass Filter Design

To ensure the triangular open-loop resonator is designed optimally, the total length was set to half the guided wavelength at the filter's center frequency. The coupling mechanism operates via the interaction of the fringe fields generated by adjacent resonators. The specific resonance configuration of the resonator in question governs the characteristics of this coupling. The design dimensions are as follows: a strip width, w, of 0.4-0.8 mm; two symmetric arms of 5.3 mm; an infinitely long horizontal base section of 11.3 mm; and a top section of 0.7 mm. The design is illustrated in figure 7.

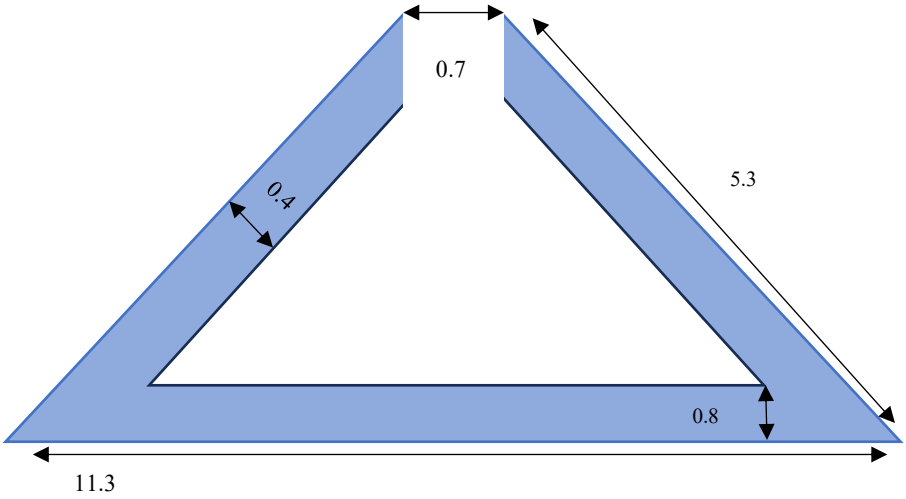

Figure 7: The proposed first suggestion resonator

Several modern filter designs hinge on different types of junctions. In this work, we examine a specific type of junction, the Stepped Impedance Resonator (SIR) junction. This type of junction can use a single resonator to create a bandpass filter (BPF), depending on the resonator's type and geometry. The design has two elongated SIR sections at the ends of each port, as shown in figure 8, which illustrates the general design of this type of filter. The SIR junction has sections of transmission line that are the same but have different characteristic impedances, providing a gradual stepwise change in impedance. The design allows energy to be transferred between the two ports via the coupling discussed in earlier sections. In Microstrip designs, the most common type of coupling is electric, or gap, coupling, which is mainly influenced by the electric field or capacitance formed between two adjacent conductive elements, such as resonators, transmission lines, and stubs. This gap is denoted by "S". Ports (Port 1 (input) & Port 2 (output), 50 Ω). These represent the input and output Microstrip feed lines.

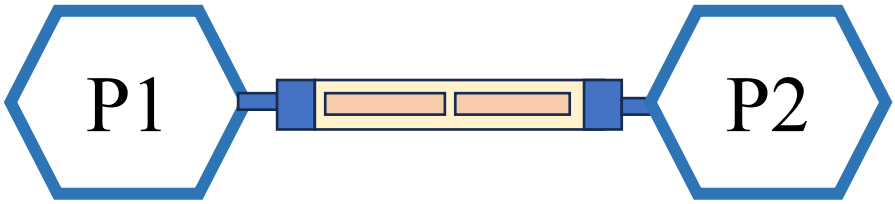

Figure 8: SIRs junction

The equivalent circuit of the electrical length and impedance for the proposed resonator, based on its length and width, is shown in figure 9.

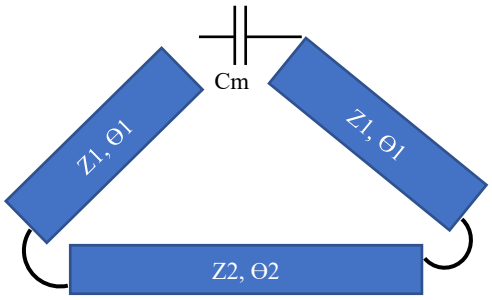

Figure 9: Equivalent circuit related by Z, Θ

The three transmission-line sections (Z1, θ1, Z1, θ1, Z2, θ2) collectively provide the distributed inductance and capacitance of the resonator loop, where Z1=145.07 Ω and Z2=116.29 Ω, resulting in width variation. The gap capacitance Cm introduces /the main electrical discontinuity, completing/ the loop and forming a resonant LC circuit with minor contributions from line-to-ground capacitances. Possible additional capacitances from line-to-ground effects.

Algorithm 1: Design Workflow for Nested Triangular CSRR-Based BPF

Input:

f_0: Target center frequency

$\varepsilon_r, h, \tan\delta$: Substrate parameters (RO3003)

Z_1, Z_2: Characteristic impedances

g: Coupling gaps

Output:

Optimized multiband microstrip bandpass filter with low insertion loss.

Pseudocode:

1. Initialize substrate and frequency specifications.
2. Design triangular resonator with electrical length $\approx \lambda_g/2$
3. Insert nested CSRR to generate additional resonant modes.
4. Assign impedance sections $Z_1$and Z_2 and set coupling gap g.
5. Simulate EM response to obtain S-parameters and group delay.
6. Optimize geometry iteratively until multiband and matching criteria are satisfied.
7. Return optimized BPF layout.

The algorithm outlines the procedure to develop a compact multiband microstrip bandpass filter using nested triangular complementary split-ring resonator (CSRR). The process starts with defining the substrate and frequency, designing a triangular open-loop resonator at the tuned guided wavelength, and integrating a nested CSRR structure to achieve a combination of electric and magnetic coupling for several resonant modes and transmission zeros. Key performance indicators are assessed using full-wave electromagnetic simulation, and a series of optimizations are employed to reduce insertion loss, improve impedance matching, and stabilize the multiband performance.

4.5 Software and Simulation Environment

Using AWR Microwave Office 15, which is a full-wave 3D EM simulation environment used to model circuits in the microwave range, the design and electromagnetics evaluation of the proposed nested triangular CSRR-based bandpass filter were completed Microwave Office Microwave circuits are modeled in a full wave EM simulation environment as the microwave circuits are modeled is as the microwave circuits are modeled as the microwave circuits are modeled as the microwave circuits are modeled as the microwave circuits are modeled as the microwave circuits are modeled as the microwave circuits are modeled as the microwave circuits are modeled as The substrate was defined using the built-in material library by selecting Rogers RO3003, with dielectric constant $\varepsilon_r = 3.0$, thickness $h = 1.52$, loss tangent $tan\ \delta = 0.0013$, and copper thickness of 35 μm.

4.6 Dataset Description

The dataset used in this work is entirely simulation-generated using the AXIEM full-wave solver in AWR Microwave Office 15. It includes frequency-domain outputs and multiple parametric variations used to evaluate and optimize the nested triangular CSRR bandpass filter. Table 1 summarizes all dataset components used for analysis and performance validation.

Table 1: Dataset used for simulation and analysis

Dataset Type	Description	Purpose in the Study
Frequency Sweep Data	Within a simulation sweep from 3 to 14 GHz with an increment of 0.005 GHz for parameters such as S11, S21, phase, group delay, and VSWR.	Models all resonances, transmission zeros, and higher-order modes with great precision.
Resonator Geometry Dataset	Changes of dimensions of an equilateral triangular resonator, including side length, base width, inner and outer resonator spacing, and top-gap size.	Assesses the effects of geometry on resonant frequency, bandwidth, and coupling strength.
Coupling Gap Dataset	Gaps of 0.1 mm to 0.7 mm between the resonator and the feedlines, as well as between the nested resonators.	Analyzes variation in external Q, hybrid electric magnetic coupling, and transmission-zero.
Microstrip Line Parameters	Variations in width to change the characteristic impedance and, therefore, the effective permittivity.	Guarantees proper matching at 50 Ω and certifies transmission-line-level performance.
Material & Substrate Dataset	RO3003 substrate with εr = 3.0, height = 1.52 mm, loss tangent = 0.001, copper thickness = 35 microns.	Provides uniform dielectric and conductor properties across all simulation runs.
Parametric Sweep Outputs	Responses of S-parameters were produced for each change of geometry and of coupling.	Determines the best arrangement for multiband operation and augmentation of selectivity.

5 Results and Discussion

Performance Metrics

The performance of the proposed bandpass filter is primarily evaluated using insertion loss and return loss derived from the simulated S-parameters. The insertion loss, which represents the signal transmission efficiency through the filter, is calculated by equation 13:

$$Insertion\ Loss\ (dB) = -20\ log_{10}|S_{21}| \quad (13)$$

The return loss, which indicates the impedance matching quality at the input port, is given by equation 14:

$$Return\ Loss\ (dB) = -20\ log_{10}|S_{11}| \quad (14)$$

These two metrics are used to assess the transmission performance and impedance matching behaviour of the proposed filter across all operating passbands.

The design and modifications of the BPFs using AWR were performed over the frequency range of 3 to 14 GHz in 0.005 GHz intervals, with the results presented in figure 10 of the New BPF design, which shows the worst selectivity. Figure 10 shows the S-parameter results, where S11 = 42.63 dB at 5.308 GHz and S21 = 0.089 dB. Because the CSRR can improve selectivity by introducing a transmission zero, we can create a second triangular resonator within the first one.

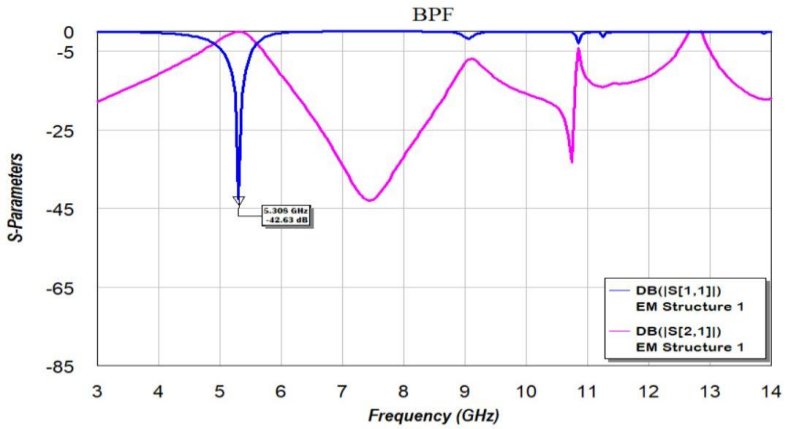

Figure 10: S-parameters for the proposed first suggestion BPF

The interval between the two ports and the external resonator is critical to the design, varying between 0.1 and 0.3, which exhibits good selectivity for the 0.1 mm gap. In contrast, for the other gap, the signal is attenuated due to an increased S11 value of -28.97, followed by the elimination of the spurious responses previously observed for the 0.1 mm gap. The spurious responses were the additional resonances found outside the passband of 5.33 GHz. They are the results from higher modes of the triangular loop and the coupling gap. Optimizing the gap size improved the filter's performance by reducing reflections, enhancing stopband suppression, and more effectively controlling spurious modes, as shown in figure 11.

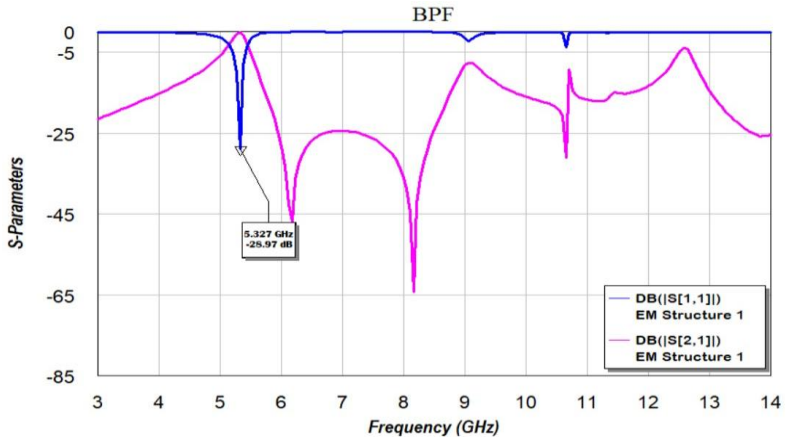

Figure 11: S-parameters for the proposed second suggestion BPF with a 0.3 gap

Finally, we show in figure 12 the optimized design using a triangular patch to reduce losses and broaden the passbands, thereby increasing the number of transmission zeros.

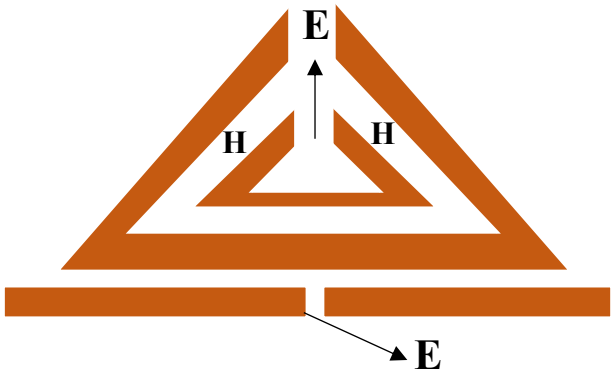

Figure 12: The proposed final suggestion BPF

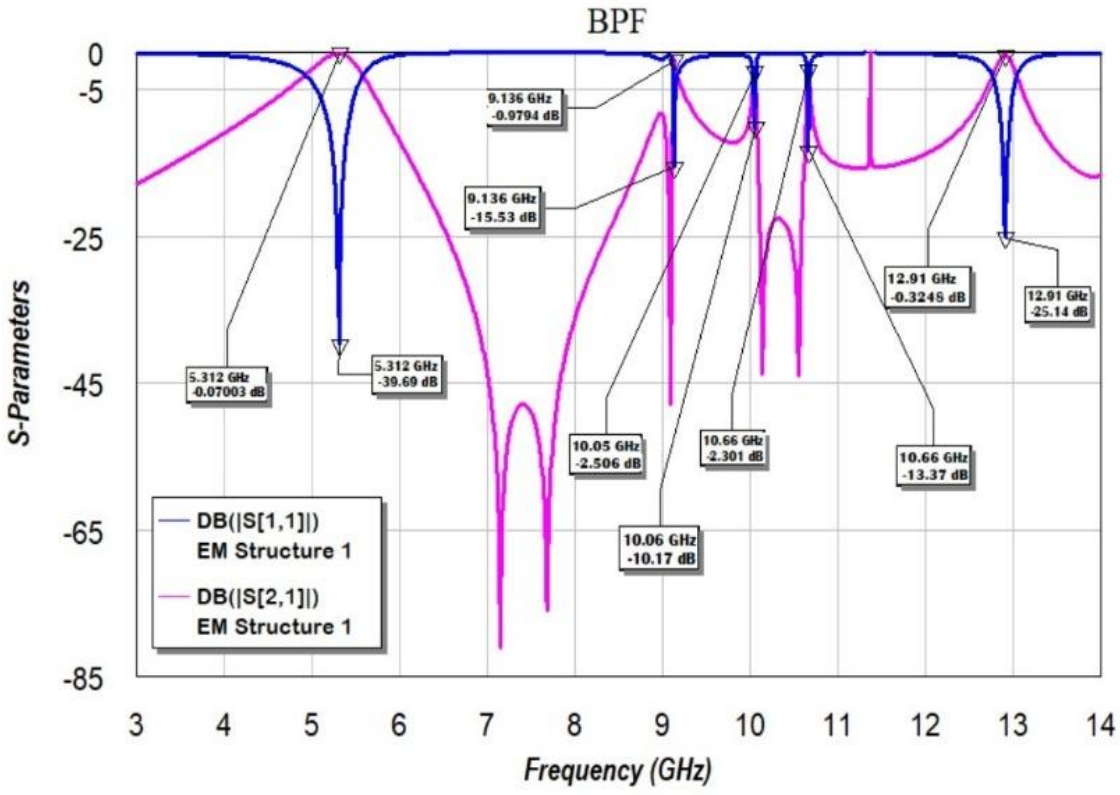

Figure 13: S-parameters of the proposed final suggestion BPF

A CSRR resonator that is nested, triangular, and designed to achieve combined electric and magnetic coupling, like the one we designed, allows for multiband operation with transmission zeros that are well-defined. As we can see in figure 13, a result of the interactions between the inner and outer resonators, multiple passbands are generated, which allows for incredible matching and a decrease in insertion loss for the primary filter in addition to a single triangular resonator design. We can see in figure 14 that the proposed BPF has a group delay with positive and negative delay regions for the

operating bands. For the negative group delay which is in the area below the zero nanoseconds line, it can be utilized in signal processing systems that are complex in order to provide the needed delay compensated system

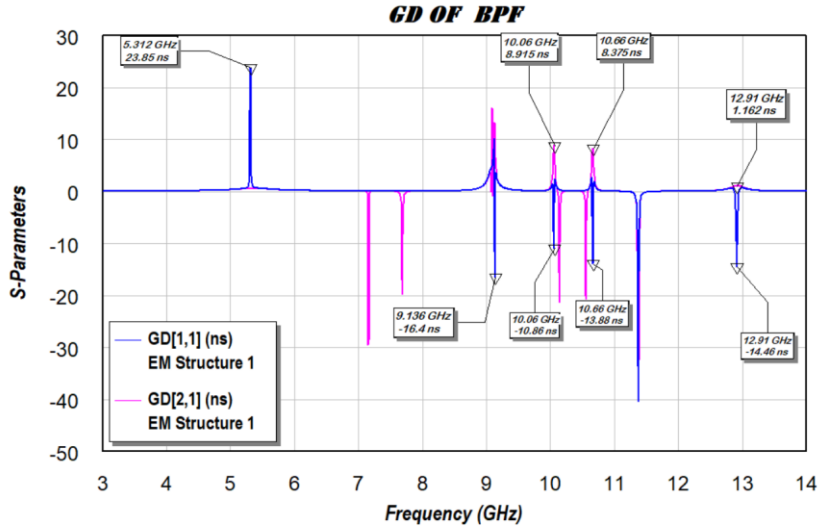

Figure 14: Group delay of Proposed final suggestion BPF

The VSWR verifies that the nested triangular CSRR filter offers impedance matching at the base frequency (5.3 GHz) and sustains resonance matching across the remaining multiband resonances (9.1, 10.0–10.6, and 12.9 GHz). All the passbands lie within the accepted VSWR range (<2), indicating optimal power transfer. Consequently, the design is successful. Figure 15 illustrates the VSWR for all passbands of the proposed final suggestion BPF (Nouri et al., 2024).

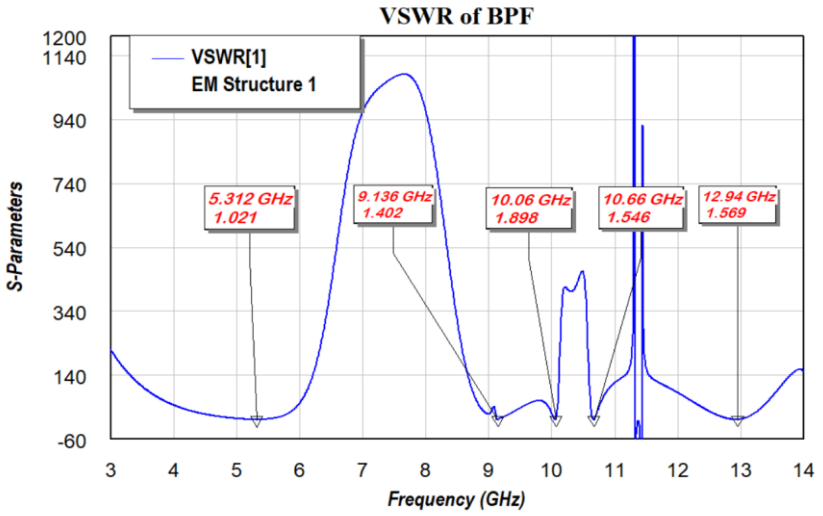

Figure 15: VSWR of proposed final suggestion BPF

The filter is seen to possess more than one resonant frequency phonon band at 5.3, 9.1, 10-10.6, 12.9 GHz. This is confirmed by the phase response, which shows a steep phase shift at the mentioned frequencies, due to resonant coupling in the triangular CSRR. The higher-order bands, in particular, have multiple abrupt phase changes, a result of the more complicated interleaving of the resonance coupling

at higher orders. The fundamental bands, however, are smoother and more phase-shiftable, reflecting the more stable coupling. The interaction between the hass responses and coupling is shown in (Li et al., 2023; Nouri et al., 2024; Al-Fatlawi et al., 2025; Kurdi et al., 2021) and figure 16. The specifications of the proposed final suggestion BPF are displayed in table 2.

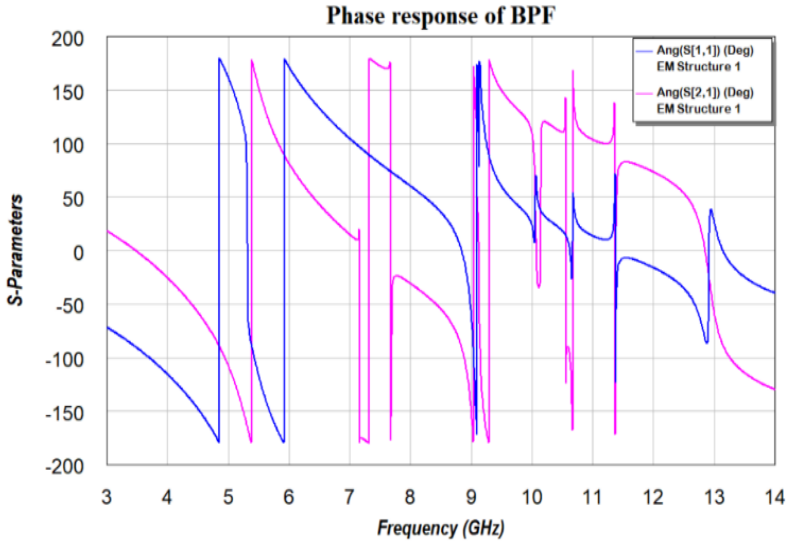

Figure 16: Phase response proposed final suggested BPF

The overall physical size of the proposed bandpass filter is 18 mm × 18 mm, corresponding to approximately 0.04 λg × 0.04 λg at the fundamental resonance. This demonstrates a high level of miniaturization compared with recently reported multiband microstrip bandpass filters. A quantitative comparison with prior works in terms of size and insertion loss is provided in table 2.

Table 2: Comparing BPF in this study with many recent studies

Ref	Center Frequency (GHz)	Return loss(dB)	Insertion loss(dB)	Size in λg × λg or mm
(Singh et al., 2025)	5.55, 7.50, 8.60	>14	1.39, 1.33, 1.53	--------
(Ren et al., 2021)	2.54, 4.62	>21	1.4, 1.95	0.69 λg× 0.76 λg
(Arunjith et al., 2021)	3.5, 4.4, 5.7	20, 14, 18	0.24, 0.45, 0.72	0.15 λg × 0.13 λg
(Massamba et al., 2022)	4.1715, 6.1425, 14.435	10	2.1, 1.3, 4.04	22.4 × 7.62 mm^2
(Xu et al., 2022)	2.91, 3.53	17, 18	1, 1.5	0.18 λg ×0.17 λg ×0.09 λg
(Basit et al., 2023)	1.57, 3.5	>25	<1.2	0.31 λg × 0.24 λg
(Ramkumar et al., 2024)	(1.67-1.97), (4.2-8.67), (9.45-10.45)	20, 15, 14	0.5, 0.2, 1	17 × 22.6 × 0.8 mm^3
(Rai et al., 2024)	1.7, 2.7, 4.5	14.95, 12.86, 17.36	1.82, 1.87, 3.4	0.35 λg × 0.28 λg
(Sekhar & Kumar, 2025)	(3411, 4190) MHz	-------	1, 0.12	40 ×300×30 mm^3
The proposed filter	5.312, 9.136, 10.06, 10.66, 12.91	**39.69, 15.53, 10.17, 13.37, 25.14**	**0.07, 0.9, 2.5, 2.3, 0.32**	**0.04** λg×**0.04** λg

6 Conclusion

In this study, a nested triangular CSRR-based bandpass filter was designed, analyzed, and benchmarked against several recently reported multiband filters. The proposed design modifies a standard triangular open-loop resonator to a small-form multiband filter model by incorporating electric and magnetic couplings. The simulation results demonstrate the realization of four distinct passbands at 5.31, 9.13, 10.0–10.6, and 12.9 GHz, with excellent return loss of -39.7 dB and very low insertion loss of 0.07 dB at the fundamental band. Compared with previously published work, the proposed filter achieves competitive, and sometimes superior, matching performance and maintains insertion loss, which is on par with or superior to a significant fraction of reported tri-band and wideband designs. Some of the references reported dual- or tri-band responses as the target of their work, and as such, employ stubs, stepped-impedance resonators, or waveguide-based structures. The triangular CSRR approach, in contrast, enables multiband operation within a more compact geometry, resulting in sharp transmission zeros. In sum, the design demonstrates that, through the deliberate arrangement of nested triangular resonators and the precise engineering of coupling slots, highly selective, low-loss, and multi-responsive BPF functionality can be achieved, applicable to modern wireless communication devices such as WLAN, WiMAX, GPS, and 5G technologies. Next steps will likely focus on miniaturization, implementation, and empirical testing to better appreciate and assess the BPF's real-world potential.

Declaration of Competing Interests

The authors declared that they have no conflicts of interest in this work.

References

[1] Ahmed, H. S., & Almamori, A. N. M. (2025). Design of a triple-band metamaterial bandpass filter utilizing modified-minkowski fractal geometry. *Progress In Electromagnetics Research C*, *154*, 159-167. https://doi.org/10.2528/PIERC25021810

[2] Al-Fatlawi, A. H., Kashef, S. S., Mezaal, Y. S., & Valizadeh, M. (2025). Design of a compact microstrip band pass filter for IoT and S-band radar applications. *Data and Metadata*, *4*, 714. https://doi.org/10.56294/dm2025714

[3] Andreica, S., Munteanu, C., Constantinescu, C., Pacurar, C., Giurgiuman, A., Gliga, M., & Dusa, S. (2024, November). Design and Simulation of Three-Band Microstrip Resonator Bandpass Filters for Wireless Communication Systems. In *IOP Conference Series: Materials Science and Engineering* (Vol. 1320, No. 1, p. 012006). IOP Publishing. https://doi.org/10.1088/1757-899X/1320/1/012006

[4] Arunjith, K. S., Ghivela, G. C., & Sengupta, J. (2021). Design and analysis of novel tri-band band pass filter for GSM, WiMax and UWB applications. *Wireless Personal Communications*, *118*(4), 3457-3467. https://doi.org/10.1007/s11277-021-08188-7

[5] Balani, W., Sarvagya, M., Ali, T., Samasgikar, A., Das, S., Kumar, P., & Anguera, J. (2021). Design of SWB antenna with triple band notch characteristics for multipurpose wireless applications. *Applied sciences*, *11*(2), 711. https://doi.org/10.3390/app11020711

[6] Basit, A., Daraz, A., Khan, M. I., Zubir, F., A. AlQahtani, S., & Zhang, G. (2023). Design and modelling of a compact triband passband filter for GPS, WiMAX, and satellite applications with multiple transmission zero's. *Fractal and Fractional*, *7*(7), 511. https://doi.org/10.3390/fractalfract7070511

[7] Chidambaram, K. R., & Rajan, P. (2025). Designing intrusion detection systems for maritime wireless sensor networks and smart port infrastructures. *Journal of Internet Services and Information Security, 15*(2), 858–870. https://doi.org/10.58346/JISIS.2025.I2.057

[8] Dawood, R. M., Shaaban, R. M., Malallah, R. E., & Ahmed, Z. A. (2025). Development and Implementation of Wideband Elliptical Ring Microstrip Antennas for 5G and X-Band Use. *Journal of Wireless Mobile Networks, Ubiquitous Computing, and Dependable Applications, 16*(1), 121-133. https://doi.org/10.58346/JOWUA.2025.I1.007

[9] Faouri, Y. S., Ahmad, S., Parchin, N. O., See, C. H., & Abd-Alhameed, R. (2022). A novel meander bowtie-shaped antenna with multi-resonant and rejection bands for modern 5G communications. *Electronics*, *11*(5), 821. https://doi.org/10.3390/electronics11050821

[10] Gari, S., Nurmantris, D. A., Ismail, N., & Munir, A. (2024, October). Development of dual-band microstrip bandpass filter based on dual-mode resonator for wireless communication applications. In *2024 IEEE Workshop on Microwave Theory and Technology in Wireless Communications (MTTW)* (pp. 113-117). IEEE. https://doi.org/10.1109/MTTW64344.2024.10742186

[11] George, A., & Iqubal, A. (2024). A review of the Design and Development of Microstrip Multiband Bandpass Filter for 5G Systems. *Journal of Applied Science, Engineering, Technology and Management*, *2*(2), 03-08. https://doi.org/10.61779/jasetm.v2i2.1

[12] Giji Kiruba, D., Benita, J., & Rajesh, D. (2023). A Proficient Obtrusion Recognition Clustered Mechanism for Malicious Sensor Nodes in a Mobile Wireless Sensor Network. *Indian Journal of Information Sources and Services, 13*(2), 53–63. https://doi.org/10.51983/ijiss-2023.13.2.3793

[13] Hasan, S. H., Hamidkhani, M., Bachache, N. K., & Mohebbi, K. (2025). Combining Transformers and Fuzzy Clustering Based on Fuzzy Functions for Optimal Uav Localization In 5g Wireless Networks. *Archives for Technical Sciences, 2*(33), 385–406. https://doi.org/10.70102/afts.2025.1833.385

[14] Kurdi, W. H. M., Rassool, H. A., & Al-fatlawi, A. H. (2021). Evaluation patterns and algorithm for cancer identifications using dynamic clustering. *Periodicals of Engineering and Natural Sciences*, *9*(2), 462-470. https://doi.org/10.21533/pen.v9.i2.755

[15] Li, C., Ma, Z. H., Chen, J. X., Wang, M. N., & Huang, J. M. (2023). Design of a compact ultra-wideband microstrip bandpass filter. *Electronics*, *12*(7), 1728. https://doi.org/10.3390/electronics12071728

[16] Mahendran, K., Gayathri, R., & Sudarsan, H. (2021). Design of multi band triangular microstrip patch antenna with triangular split ring resonator for S band, C band and X band applications. *Microprocessors and Microsystems*, *80*, 103400. https://doi.org/10.1016/j.micpro.2020.103400

[17] Mariselvam, V., Preethi, A. A. P., & Akilarasu, G. (2022). Etched triangle resonator dual band microstrip band pass filter. *Wireless Personal Communications*, *125*(2), 1537-1544. https://doi.org/10.1007/s11277-022-09620-2

[18] Massamba, O. C., Mpele, P. M., Mbango, F. M., & Lilonga-Boyenga, D. (2022). Tri-band bandpass filter using mixed short/open circuited stubs and Q-factor with controllable bandwidth for WAS, ISM, and 5G applications. *Progress in Electromagnetics Research C*, *119*, 177-190. http://dx.doi.org/10.2528/PIERC22012713

[19] Mezaal, Y. S., & Al-Zayed, A. S. (2019). Design of microstrip bandpass filters based on stair-step patch resonator. *International Journal of Electronics*, *106*(3), 477-490. https://doi.org/10.1080/00207217.2018.1545144

[20] Muhammad, F., & Sohail, K. (2022). Multi-Band Bandpass Filter Using Novel Topology for Next-Generation IoT Wireless Systems. *CMC-Computers, Materials & Continua*, *73*(3), 4819-4832.

[21] Muralidharan, J. (2023). Innovative RF design for high-efficiency wireless power amplifiers. *National Journal of RF Engineering and Wireless Communication*, *1*(1), 1-9.

[22] Mushtaq, B., & Khalid, S. (2023). Design of miniaturized single and dual-band bandpass filters using diamond-shaped coupled line resonator for next-generation wireless systems. *International Journal of Microwave and Wireless Technologies*, *15*(3), 375-383.

[23] Nouri, L., Nkenyereye, L., Hafez, M. A., Hazzazi, F., Chaudhary, M. A., & Assaad, M. (2024). A simplified and efficient approach for designing microstrip bandpass filters: Applications in satellite and 5G communications. *AEU-International Journal of Electronics and Communications*, *177*, 155189. https://doi.org/10.1016/j.aeue.2024.155189

[24] Oleiwi, N. R., & Hasan, M. F. (2025, February). A quad-band highly selective miniaturized microstrip band-pass filter design based on multi-fractal geometry for wireless applications. In *AIP Conference Proceedings* (Vol. 3169, No. 1, p. 040075). AIP Publishing LLC. https://doi.org/10.1063/5.0254299

[25] Pandey, P., Pandey, A. K., & Chauhan, R. K. (2022). Novel Tri-band Microstrip Bandpass Filter with Stub Loaded in Circular Ring Resonator. In VLSI, Microwave and Wireless Technologies: Select Proceedings of ICVMWT 2021 (pp. 357-366). Singapore: Springer Nature Singapore. https://doi.org/10.1007/978-981-19-0312-0_36

[26] Rai, J. K., Choudhary, D. K., Ranjan, P., & Chowdhury, R. (2024). A compact ultrawide bandpass filter along Notch characteristics with rectangular resonator through a machine learning approach. *International Journal of Microwave and Wireless Technologies, 16*(8), 1414-1422.

[27] Ramkumar, S., Saravanan, M., Nyruthi, A. K., Nishanthan, M., Kiruthika, V. M., & Anitha, M. (2024, December). Compact Triple-Band Bandpass Filter Using Coupled Resonators with Transmission Zeros. In *2024 IEEE Microwaves, Antennas, and Propagation Conference (MAPCON)* (pp. 1-5). IEEE. https://doi.org/10.1109/MAPCON61407.2024.10923220

[28] Rehman, M. A., Mushtaq, B., Khalid, S., & Rehman, M. U. (2024). Design of a miniaturized multi resonance resonator based highly selective dual wideband bandpass filter. *Microelectronics Journal*, *153*, 106411. https://doi.org/10.1016/j.mejo.2024.106411

[29] Ren, B., Liu, X., Guan, X., Xu, M., & Zhang, Z. C. (2021). A dual-wideband balanced bandpass filter based on branch-line structure with controllable common-mode suppression. *Frontiers in Physics*, *9*, 764648. https://doi.org/10.3389/fphy.2021.764648

[30] Rezaei, A., Yahya, S. I., Noori, L., & Jamaluddin, M. H. (2022). Designing high-performance microstrip quad-band bandpass filters (for multi-service communication systems): A novel method based on artificial neural networks. *Neural Computing and Applications*, *34*(10), 7507-7521. https://doi.org/10.1007/s00521-021-06879-7

[31] Sekhar, M., & Kumar, L. (2025, January). Spiral ring resonator-based dual-band waveguide BPF for satellite CDMA signal tracking in a 5G environment. In *2025 8th International Conference on Electronics, Materials Engineering & Nano-Technology (IEMENTech)* (pp. 1-5). IEEE. https://doi.org/10.1109/IEMENTech65115.2025.10959618

[32] Sharma, U., Srivastava, G., Khandelwal, M. K., & Roges, R. (2024). Design Challenges and Solutions of Multiband MIMO Antenna for 5G/6G Wireless Applications: A Comprehensive Review. *Progress in Electromagnetics Research B*, *104,* 69-89. http://dx.doi.org/10.2528/PIERB23101904

[33] Singh, C., Sharma, C., & Kumar, A. (2025). Miniaturized Ultra-Wideband microstrip antenna with triple band-notched characteristics at WiMAX/WLAN/X-band for medical applications. *Physica Scripta*, *100*(5), 055523. https://doi.org/10.1088/1402-4896/adc6d0

[34] Slimani, A., Das, S., Ali, W. A. E., El Alami, A., Bennani, S. D., & Jorio, M. (2022). Second order microstrip bandpass filter design based on square resonator for 5G sub-6 GHz band. *Journal of Instrumentation*, *17*(07), P07002. https://doi.org/10.1088/1748-0221/17/07/P07002

[35] Weng, X., Xu, K. D., & Fan, H. (2023). Wideband bandpass filters based on eighth-mode substrate integrated waveguide and microstrip resonators. *IEEE Transactions on Circuits and Systems II: Express Briefs*, *70*(7), 2375-2379. https://doi.org/10.1109/TCSII.2023.3244791

[36] Xu, Z., Wu, Y., Dong, Q., & Wang, W. (2022). Miniaturized dual-band filter using dual-mode dielectric waveguide resonator. *IEEE Microwave and Wireless Components Letters*, *32*(12), 1411-1414. https://doi.org/10.1109/LMWC.2022.3193424

[37] Yahya, S. I., Zubir, F., Nouri, L., & Jizat, N. M. (2024). An ultra-compact microstrip bandpass filtering coupler with suppressed harmonics and low group delay: a novel structure for 5G applications. *Results in Engineering*, *24*, 103003. https://doi.org/10.1016/j.rineng.2024.103003

Authors Biography

Mustafa Abd Al-Aress Jabur received the B.Sc. degree in Electrical Engineering from the University of Kufa and the M.Sc. degree in Electronic Engineering from the University of Technology, Baghdad, Iraq, in 2013 and 2017, respectively. He received the Ph.D. degree in communication system engineering from the University of Urmia, Iran, in 2025. He is now a lecturer in Computer Technical Engineering at Imam Kadhum University College, Iraq. His research interests include wireless communication, antenna design, optical fiber communication, optical sensors, and signal processing.

Rami Qays Malik was born in Babylon, Iraq. He completed his secondary school at several schools in AL Hilla, Babylon, Iraq. He pursued his degree at Al-Furat Al-Awsat Technical University in Iraq and graduated with a B.Eng. in Communication Engineering in 2011. Then, he was enrolled in the M.Tech program at the Department of Electronics and Communication, Sam Higginbottom, University of Agriculture, Technology and Sciences, Allahabad, India, in 2012. Accordingly, in January 2014, Mr. Rami pursued a master's degree in optical fibre communication. Thereafter, he was appointed as a lecturer at AL-Mustaqbal University College, Babylon, Iraq. In October 2017, the author was pursuing a Ph.D. in Electrical Engineering at the Faculty of Electrical and Electronic Engineering, Universiti Tun Hussein Onn Malaysia (formerly known as Institute Technology Tun Hussein Onn), 86400 Parit Raja, Batu Pahat, Johor, Malaysia. During this time, Mr. Rami has been the primary author of many academic papers in the field of communication engineering. He obtained his Ph.D. in 2021 and currently serves as a lecturer at AL-Mustaqbal University, where he also serves as coordinator of the Medical Instrumentation Department.

Zahraa Hashim Kareem were born in Babylon, Iraq. She pursued her degree at Babylon University in Iraq and graduated with a B.Eng. in Electrical Engineering in 2012. Thereafter, she was appointed as an engineer at Babylon University. In 2014, she joined the Electronic and Communication Department at the College of Electrical Engineering at the University of Babylon, Iraq. In September 2016, Mrs. Zahraa pursued her higher education by enrolling in a Master's program in Wireless Telecommunication. Following her graduation, she was appointed as a lecturer at AL-Mustaqbal University College, Babylon, Iraq. In October 2017, she commenced her Ph.D. in Electrical Engineering at the Faculty of Electrical and Electronic Engineering, Universiti Tun Hussein Onn Malaysia (formerly known as Institute Technology Tun Hussein Onn) in Batu Pahat, Johor, Malaysia. During this period, Mrs. Zahraa became the lead author for many academic papers in the field of communication engineering. She obtained her Ph.D. in 2021 and currently serves as a lecturer at AL-Mustaqbal University, where she also serves as Director of the Quality Assurance and Academic Performance Department.

Aqeel H. Al-fatlawi was born in Babylon, Iraq. He completed his secondary school at several schools in Al-Diwaniya, Iraq. He pursued his degree at Al-Furat Al-Awsat Technical University in Iraq and graduated with a B.Eng. in Communication Engineering in 2011. Then, in 2012, he enrolled in the M.Tech program in the Department of Electronics and Communication Engineering at Sam Higginbottom University of Agriculture, Technology and Sciences, Allahabad, India, completing his master's degree in 2014. Dr. Al-fatlawi pursued his Ph.D. in Wireless Communication at Urmia University, IRAN, obtaining his degree in 2025. He has authored many academic papers in the areas of communication engineering. He

currently serves as an Assistant Professor at Imam Kadhum College. His research interests include microstrip design, antennas, filters, diplexers, and triplexers.

Ahmed R. Mathloom, Teaching at the University of Dhi Qar, Faculty of Education, Drainage Department of Physics, Doctoral Certificate, General Jurisdiction of Physics Sciences with Mactical Jurisdiction of Medical Physics in 2021 from the University of Basra, and the Scientific title Assistant Professor in 2022. I have published a lot of scientific research, as well as taught and supervised graduate students.

Amjed Abbas Ahmed Center for Cyber Security, Faculty of Information Science and Technology Universiti Kebangsaan Malaysia, Bangi, Malaysia Department of Computer Techniques Engineering, Imam AlKadhum College (IKC), Baghdad, Iraq.